Solid Earth Discuss., 6, 145–190, 2014
www.solid-earth-discuss.net/6/145/2014/
doi:10.5194/sed-6-145-2014
© Author(s) 2014. CC Attribution 3.0 License.

Solid Earth
Discussions
Open Access

This discussion paper is/has been under review for the journal Solid Earth (SE).
Please refer to the corresponding final paper in SE if available.

Pacific Plate slab pull and intraplate deformation in the early Cenozoic

N. P. Butterworth[1], R. D. Müller[1], L. Quevedo[1], J. M.O'Connor[2], K. Hoernle[3], and G. Morra[4]

[1]EarthByte Group, School of Geosciences, The University of Sydney, New South Wales, 2006, Australia
[2]GeoZentrum Nordbayern, Erlangen and Alfred Wegener Institute for Polar and Marine Research, Bremerhaven, Germany
[3]GEOMAR Helmholtz Centre for Ocean Research Kiel, Germany
[4]Department of Physics and School of Geosciences, University of Louisiana at Lafayette, 70504, LA, USA

Received: 22 December 2013 – Accepted: 23 December 2013 – Published: 14 January 2014

Correspondence to: N. P. Butterworth (nathaniel.butterworth@sydney.edu.au)

Published by Copernicus Publications on behalf of the European Geosciences Union.

Abstract

Large tectonic plates are known to be susceptible to internal deformation, leading to a range of phenomena including intraplate volcanism. However, the space and time dependence of intraplate deformation and its relationship with changing plate boundary configurations, subducting slab geometries, and absolute plate motion is poorly understood. We utilise a buoyancy driven Stokes flow solver, BEM-Earth, to investigate the contribution of subducting slabs through time on Pacific Plate motion and plate-scale deformation, and how this is linked to intraplate volcanism. We produce a series of geodynamic models from 62 to 42 Ma in which the plates are driven by the attached subducting slabs and mantle drag/suction forces. We compare our modelled intraplate deformation history with those types of intraplate volcanism that lack a clear age progression. Our models suggest that changes in Cenozoic subduction zone topology caused intraplate deformation to trigger volcanism along several linear seafloor structures, mostly by reactivation of existing seamount chains, but occasionally creating new volcanic chains on crust weakened by fracture zones and extinct ridges. Around 55 Ma subduction of the Pacific-Izanagi ridge reconfigured the major tectonic forces acting on the plate by replacing ridge push with slab pull along its north-western perimeter, causing lithospheric extension along pre-existing weaknesses. Large scale deformation observed in the models coincides with the seamount chains of Hawaii, Louisville, Tokelau, and Gilbert during our modelled time period of 62 to 42 Ma. We suggest that extensional stresses between 72 and 52 Ma are the likely cause of large parts of the formation of the Gilbert chain and that localised extension between 62 and 42 Ma could cause late-stage volcanism along the Musicians Volcanic Ridges. Our models demonstrate that early Cenozoic changes in Pacific plate driving forces only cause relatively minor changes in Pacific absolute plate motions, and cannot be responsible for the Hawaii-Emperor Bend (HEB), confirming previous interpretations that the 47 Ma HEB does not reflect an absolute plate motion event.

SED
6, 145–190, 2014

1 Introduction

The origin of intraplate volcanism without age progression and far away from plate boundaries is poorly understood (Lee and Grand, 2012; Koppers, 2011). Intraplate volcanism can be viewed as being due to hotspots within tectonic plates, which may be caused by a range of processes including mantle plumes, small-scale convection, or lithospheric extension of plates (Ito and van Keken, 2007). In an effort to categorize these phenomena Courtillot et al. (2003) distinguished three categories of hotspots. The first is the classic Wilson-Morgan type mantle plume (Morgan, 1971; Wilson, 1963), a thermal anomaly rising through the mantle due to the density difference between the core-mantle boundary and the surface. These are often long-lived and have a relatively stable source location. The second type is similar, but originates from the bottom of the transition zone, associated with superswells (Koppers et al., 2003; Romanowicz and Gung, 2002), and is comparatively short-lived. The third type (Liu and Stegman, 2012; Ito and van Keken, 2007; Hirano et al., 2006; Koppers et al., 2003) is the most broadly classified hotspot, potentially caused by many factors, and the use of the term hotspot to describe this type of volcanism can be a misnomer. The melting anomaly may not be necessarily hot (Bonatti, 1990) and may not be a singular spot (Sandwell and Fialko, 2004). It has been suggested (Ballmer et al., 2013; Conrad et al., 2011) that shear mantle flow within the asthenosphere mostly explains this type of intraplate volcanism. However, lithospheric extension driven by plate boundary forces, plate motion, and small-scale covection may be causing intraplate volcanism as well (Ballmer et al., 2009; Koppers et al., 2003; Sandwell et al., 1995). Lithospheric cracking due to plate flexure (Hirano et al., 2006) and thermal contraction (Sandwell and Fialko, 2004) is also a possible contributor to surface volcanics. The cracking hypothesis presumes pre-existing partial melt below the surface that may be erupted when stress is applied (Ballmer et al., 2009; Hieronymus and Bercovici, 2000). Intraplate magmatism may occur in conjunction with classic hotspot volcanism, and may be associated with highly strained areas overlapping pre-existing zones of weakness (Davis et al., 2002;

SED
6, 145–190, 2014

Staudigel et al., 1991) or may create new weak zones that give rise to volcanism. Most intraplate volcanism occurs along pre-existing tectonic fabric or around highly stressed lithosphere (Clouard and Gerbault, 2008a).

Here we investigate how intraplate deformation in the oceanic lithosphere may be caused by subduction driven plate dynamics, how this deformation might contribute to the occurrence and timing of volcanic melting anomalies, and to what extent intraplate volcanism may leave the lithosphere more susceptible to the passage of future melts (Hillier, 2007), focussing on the Pacific Plate evolution in the early Cenozoic. This time period captures the major global tectonic plate reorganisation between 53–50 Ma (Cande and Stegman, 2011; Whittaker et al., 2007) during a period of heterogenous plate tessellation (Morra et al., 2013). Large plate accelerations have been shown to lead to increased volcanic flux (Hieronymus and Bercovici, 2000; Anderson, 1994), therefore the analysis of the early Cenozoic is a good candidate for a relatively active volcanic period. We analyse changes in plate motion around the Pacific ocean basin by considering slab-pull and mantle drag/suction forces and compare the results with absolute plate reconstructions (Seton et al., 2012; Doubrovine et al., 2012; Chandler et al., 2012; Wessel and Kroenke, 2008) and the occurrence of intraplate volcanics (e.g. Clouard and Bonneville, 2005).

2 Model setup

We apply a novel workflow utilising a Stokes flow solver, BEM-Earth (Quevedo et al., 2012a; Butterworth et al., 2012; Morra et al., 2012, 2007), to analyse the coupled plate-mantle dynamics in the Late Cretaceous and early Cenozoic. Our model is driven by upper mantle slab-pull buoyancy forces and by induced slab-suction from the down-going plates, similar to previous work (Faccenna et al., 2012; Conrad and Lithgow-Bertelloni, 2004, 2002). A BEM-Earth simulation requires a set of rheological isosurfaces (here represented by the lithospheric plates, the core, and the external Earth surface). Each isosurface bounds a homogenous region characterised by an effective

SED
6, 145–190, 2014

density and viscosity. In our models these are defined by the surface location of the Pacific, Izanagi, Farallon, and Kula plates and their attached lithosphere and subducting slabs (Fig. 1).

The location of the plates and subducting slabs, used as an initial model starting condition, are determined using tectonic reconstructions from Seton et al. (2012) as implemented in the GPlates software (Boyden et al., 2011). We use reconstructed topologically closed plate boundaries through time, along with modelled plate lithospheric thickness to produce a three-dimensional representation of the Pacific Plate through time. Oceanic lithosphere thickness is derived from the reconstruction model along with oceanic paleo-age grids with a $1^\circ \times 1^\circ$ resolution (Müller et al., 2013). Ages are input into a half-space cooling model to determine plate thickness, as used previously in BEM-Earth (Morra et al., 2012, Appendix B).

We utilise 10 million years of subduction history, from plate kinematic reconstructions, to provide an estimate of slab material that drives the slab-pull force in BEM-Earth. A 10 million year interval reflects the approximate time for a slab to subduct to the lower mantle and thus represents the portion of the slab contributing to the slab-pull (Billen, 2008). To determine initially subducted slab morphology we advect subducting plates into the mantle using surface plate kinematics based on published plate rotations (Seton et al., 2012) starting 10 Myr before the geodynamic model starting time. The absolute and convergent velocities are determined for each point along the reconstructed subduction zone for each time period (Quevedo et al., 2012b). Absolute motions define the surface rotation of the slab's position and the convergence defines the upper mantle slab sinking rate. The initial dip of the slab does not affect the BEM-Earth simulation (Morra et al., 2012), but rather having the correct amount of upper mantle slab material (Quevedo et al., 2012b; Billen, 2008; Schellart, 2004) is important for simulating driving forces. Nevertheless, resulting dips for a test case of present day slab material are comparable with Slab1.0 (Hayes et al., 2012, Appendix A). At each reconstructed point, we calculate the volume of the slab driving the model, as the convergence rate

SED
6, 145–190, 2014

times the lithospheric thickness added up in 1 Myr time steps for the 10 Myr prior to the model start time.

The resulting modelled plate consists of a mantle viscosity and density structure that is post-processed to ensure smooth non-overlapping 3-D surfaces. This is required to maintain a consistent isostatic equilibrium between the model isosurfaces (Butterworth et al., 2012; Morra et al., 2012).

Rheology of the plate is defined by an isosurface bounding a region of homogenous density and viscosity (as described in Table 1). The simplified rheology structure is free to deform visco-plastically, and is a fair representation for modelling plate-scale lithospheric processes (Li and Ribe, 2012; Capitanio et al., 2010). Each subducting plate is embedded in a homogenous mantle fluid surrounded by an adaptive external surface. A mantle with no viscosity layering simplifies our model, however the role of mantle layering influences the trench morphology (Morra et al., 2012) but would not affect the plate motions and intraplate deformation.

Resolution of the model is determined by the number of triangular elements (panels) making up each rheological isosurface, which is ~ 50 km. Evolution of the model is driven by the negative buoyancy of the already-subducted lithosphere. As no lithosphere is being replenished at the mid ocean ridges, we only run the model for a few million years at a time to obtain the intraplate deformation and velocities of the plates. The tapered lithospheric thickness at the ridges of the model isosurfaces prompts a ridge-push force to contribute to plate motion, however, the force is diminished by a "surface contact layer" (Butterworth et al., 2012; Morra et al., 2012). The contact layer keeps the plates in isostatic equilibrium by preventing the slab from detaching from the external Earth surface boundary and sinking vertically; rather the subducting plate advances in a more realistic fashion. There are several methods for providing this balancing buoyancy force in numerical models (Ribe, 2010; Stegman et al., 2010; Morra et al., 2007). Here we use a "lubrication layer" method, where the Earth surface boundary is described as an adaptive surface, whose dynamic behaviour is controlled partially by the distance between the model isosurfaces. The ridge-push force con-

SED
6, 145–190, 2014

tributes less than 10 % (Lithgow-Bertelloni and Richards, 1998) to forces driving plate motions, in BEM-Earth models we find this force contributes less than 5 % due to the contact layer overwhelming the interaction (Butterworth et al., 2012).

2.1 Plate deformation

We extend the work of Clouard and Gerbault (2008a) into a 3-D spherical domain, where we examine intraplate deformation driven by plate-scale tectonics and its relationship to volcanism. However, we use a dynamic simulation with no external velocity forcing. The natural strains, ϵ, are calculated for each model panel through time using $\epsilon = \frac{L}{\ell} - 1$, where L and ℓ are the original and final lengths of model panels respectively. Principal axis stresses are then computed from the natural strains and strain rosette gauge transformation tensors. Finally, the von Mises Criterion, which is an effective or equivalent stress that can be used as measure of deformation (Gueydan et al., 2008), is defined in three dimensions as $\sigma_e = \frac{1}{\sqrt{2}}\sqrt{(\sigma_1 - \sigma_2)^2 + (\sigma_2 - \sigma_3)^2 + (\sigma_3 - \sigma_1)^2}$, where σ is the principal stress in each of the 3 axes (Boresi and Schmidt, 2003).

The plate with a simplified rheology is free to deform visco-plastically due to forces driving the natural evolution and transmission of stresses in the plate. Deformation is determined over a phase of steady model evolution after a period of initialisation. This delay in measurement allows the model to equilibrate. However, results are found to be similar when the deformation is measured early or later in the simulation. Pre-existing zones of weakness (e.g. fracture zones) likely act as conduits for melting anomalies (Davis et al., 2002), but plate-scale deformation due to subduction processes may provide the stresses required to promote volcanics. Volcanism is not expressed in the models, but we use $^{40}Ar/^{39}Ar$ for the relatively few samples available from seafloor volcanism edifices, to see if a link can be established in some places between subduction-driven plate deformation and spatio-temporal localisation of hotspot melting anomalies.

SED
6, 145–190, 2014

3 Model results

We run four subduction driven models which start with surface reconstructions at 62, 52, 47, and 42 Ma and include the previous 10 million years of subduction material as an initial condition. The resulting model deformation is correlated with age-dated volcanic structures, and the model kinematics are compared with alternative plate model reconstructions.

3.1 62 Ma reconstruction

The reconstructed Pacific Plate at 62 Ma (Fig. 2) only has one subducting slab mechanically attached to it, along the East Junction subduction zone, located to the north of Australia between the Tethys and Panthalassa (Seton and Müller, 2008). Slab-pull and basal drag (due to induced slab-suction) are the only significant model driving forces (Morra et al., 2012; Butterworth et al., 2012). At this time, the pull due to Junction slab attached to the Pacific only originates from ∼ 4 % global slab material. The subducting plates, Izanagi, Kula, and Farallon, that surround the Pacific have subduction zones with over 70 % of global slab material driving them. Reconstructed Pacific Plate velocities from Seton et al. (2012) show the plate heading toward the north-west (303°). The Doubrovine et al. (2012) reconstructions have the Pacific moving generally toward the north (15°). The Izanagi, Kula, and Farallon plates maintain the dominant subducting slabs around the Pacific. The direction of movement of the modelled Pacific (287°) is more inline with those predicted by the Seton et al. (2012) reconstructions. We observe the deformation on the plate at 62 Ma to be more contrasting across the plate with a large zone of focussed deformation running from the centre of the Pacific to the north-west intersection with the Izanagi plate.

SED
6, 145–190, 2014

3.2 52 Ma reconstruction

Between 62 and 52 Ma the Pacific Plate model undergoes a relatively major change in its kinematics and topology (Fig. 3). The Izanagi plate is now fully subducted and its subducting slab is fully coupled with the north-west portion of the Pacific Plate. Subducting slabs attached to the Pacific Plate now account for ∼ 24 % of global material being subducted. The Farallon and Kula plates have down-going material accounting for ∼ 24 % and ∼ 12 % of global material respectively. This induces high strain just behind the subduction zone in the down-going Pacific Plate. This high-strain region feeds into the same north-west trending feature seen at 62 Ma that tapers off toward the centre of the plate. There are also smaller zones of high-strain scattered around the plate. The modelled velocities show the Pacific moving westerly (280°), and rotating clockwise. As subduction is now the major driver of the Pacific Plate, the model velocity vectors are more consistent with the direction of the velocities of Seton et al. (2012) (293°). In the model the velocities are exaggerated close to the subduction zone. The Doubrovine et al. (2012) velocities have increased in magnitude and show the Pacific moving more westerly (337°), similar to the Seton et al. (2012) reconstructions during this epoch. Doubrovine et al. (2012) reconstructions favour a more northward trend to our model velocities and the Seton et al. (2012) reconstructions.

3.3 47 Ma reconstruction

The Pacific Plate approaches periods of rapid change in the Seton et al. (2012) reconstruction between 52 and 42 Ma. We run a model in the intervening period at 47 Ma to capture this change. At this time (Fig. 4) the major subduction zone attached to the Pacific is only along the west and north-west region, now accounting for ∼ 15 % of global slab material, topologically similar to the 52 Ma model. The other major dynamic influences come from the Kula and Farallon plates and their attached subducting slabs, which account for ∼ 16 % and ∼ 33 % of global slab material respectively. The Pacific Plate in our model is now moving in a predominantly westerly direction (283°) and

SED
6, 145–190, 2014

has slowed corresponding with a decrease in assumed depth of initial slab material. The large subducting slab attached to the Pacific Plate is the main driver of plate motion in this epoch. The model and reconstructed velocity vectors of Seton et al. (2012) (288°) agree well overall. Doubrovine et al. (2012) plate velocities trend more to the north (341°) and the magnitude has decreased significantly since 52 Ma. Deformation in the plate has similar style to the 52 Ma model, with patches of high-strain appearing over the plate or propagating from the edges; however, the large region of deformation propagating from the north-west subduction zone has been greatly dissipated.

3.4 42 Ma reconstruction

The modelled Pacific at 42 Ma (Fig. 5) is kinematically and topologically similar to the 47 Ma model. The same subduction zones continue to drive the Pacific as from the 47 Ma model epoch. The model direction vectors (288°) have the same north-west trend as the Seton et al. (2012) reconstructed plate motion vectors (294°). Doubrovine et al. (2012) reconstructions show the Pacific undergoing an apparent motion change, trending from north at 47 Ma to now north-west (310°). There is a correspondence between the two kinematic reconstructions and our model, with all models bearing predominately toward the west and north. The areas of high-strain are maintained in similar locations to 47 Ma.

4 Discussion

4.1 Kinematic vs. geodynamic model plate motions

From Seton et al. (2012) reconstructions, there are abrupt motion changes in the Pacific Plate between 60 and 59 Ma, 56 and 55 Ma, 50 and 49 Ma, and also between 48 and 47 Ma. These are captured between the 62 Ma and 52 Ma, and the 52 Ma and 47 Ma models respectively (Figs. 2–4). However, our models cannot capture changes over time periods in between model runs.

SED
6, 145–190, 2014

The plates in our geodynamic model are primarily driven by slab material pulling on a given attached plate. Contributions of induced mantle flow, expressed as a suction force, are secondary to this, but can still be appreciable, depending on the location of the slabs relative to the plates (Morra et al., 2012). The slab-suction force is driven from the slabs attached to the down-going plates, but we do not model the effect of tractions that may be induced by other density heterogeneities in the mantle (Ricard et al., 1993). The role of slab-suction is most evident in the motion of the 62 Ma Pacific, where the plate has no major subduction zones, but continues to move towards the north-west as predicted by kinematic reconstructions (Seton et al., 2012). At times when the large subduction zones bound the Pacific Plate, motion in our model is well constrained and our velocity directions are consistent with kinematically derived plate motions of Seton et al. (2012). However, the magnitudes of our modelled velocities are unrealistically amplified near major subduction trenches as that portion of the slab begins to rapidly descend, as such we normalise the vectors to the maximum velocity predicted by the kinematic reconstructions (Morra et al., 2012).

The correspondence between the model velocities favouring Seton et al. (2012) over Doubrovine et al. (2012) derived velocities, are in-part because the Doubrovine et al. (2012) plate model has been constructed to include Pacific hotspots that mimic the Hawaiian-Emperor bend. However, because this hotspot track is uniquely related to mantle flow (Sharp and Clague, 2006), perhaps involving ridge-plume capture (Tarduno et al., 2009), we find our subduction driven model better fits Seton et al. (2012) (based on the hotspot moving reference frame of O'Neill et al., 2005) reconstructions.

Furthermore, between 83.5 and 45 Ma the Seton et al. (2012) and Doubrovine et al. (2012) plate motions are constrained using different plate circuits. Between 50–70 Ma there is a large transition in the absolute plate motion of the Doubrovine et al. (2012) model attributed to the fast motion of the Indian plate. This could be a point of model velocity mismatch, as our models do not include plates far from the Pacific.

To further constrain the reliability of our plate motions we compare the Euler poles of the Pacific Plate for each model time with four different plate reconstructions along

SED
6, 145–190, 2014

with our subduction driven BEM-Earth model (Fig. 6). The location of the Euler pole quantifies the direction of rotation for a given plate and thus provides a good measure of correspondence between alternate models. For the time period modelled here (62–42 Ma) Wessel and Kroenke (2008) determines plate motions by assuming fixed hotspots in the Pacific. They determine Pacific rotations directly from an absolute reference frame. Alternatively Doubrovine et al. (2012) applies a moving Pacific, Atlantic, and Indian hotspot model, with rotations of the Pacific linked through a plate circuit to the absolute reference frame. Euler poles determined from Chandler et al. (2012) and Seton et al. (2012) are strikingly similar in absolute motion through time as both models rely on a moving Indian/Atlantic hotspot reference frame (O'Neill et al., 2005), and both link their plate circuits to Africa. They deviate from each other after 47 Ma as Chandler et al. (2012) interprets the rapid change in Pacific plate motion expressed in the Hawaiian-Emperor bend as being due to a slowdown in drift of the Hawaiian plume.

Each of the four plate reconstruction models sustain a sharp transition between 52 and 62 Ma, indicating a significant motion change in the Pacific. The poles associated with the dynamically modelled Pacific also capture this motion change, revealing that the subducting slab topology is congruent in influencing plate motion changes. The disparity of the Wessel and Kroenke (2008) poles from the other models highlights the impact of including fixed Pacific hotspots in plate reconstructions without considering differential hotspot motion or seamounts offset from hotspot locations. Our dynamically modelled motions of the Pacific Plate, which are agnostic of mantle plumes and plume drift, are reliant on the approach used for a given plate reconstruction methodology, as the plate model used determines the amount and location of slab material in the upper mantle. The overall good correspondence between the absolute plate velocities of the reconstruction used to build our simulation (Seton et al., 2012) and the slab driven model prediction provides the insight that a combined relative/absolute plate motion model built without relying on Pacific hotspot tracks, and particularly not the Hawaiian-Emperor chain, predicts kinematic absolute Pacific plate velocities that are plausible based on a subduction-driven dynamic model. This confirms the view that

SED
6, 145–190, 2014

the Hawaiian-Emperor bend does not reflect a change in absolute (or relative) plate motion, but that it is due to the slowdown of the drift of the Hawaiian plume (Tarduno, 2007; Tarduno et al., 2009).

4.2 Subduction zone topologies driving plate deformation

Location and amount of slab material along subduction zones determines the direction and magnitude of plate motion. Tectonic plates do not move completely rigidly but are free to deform according to the interaction and relative contribution of the slab-pull force, induced suction forces, and basal drag forces over the entire plate. In our models magnitudes of the non-dimensional deformation, represented by the von Mises, are derived from the change in length of the plate panels and the interval of time steps that the model is run for. The higher the von Mises the more likely the plate will yield, in reality this will occur dependent on the rheological properties of the lithosphere.

At 62 Ma there is an absence of any major subduction zones driving Pacific Plate motion and deformation. For this modelled time significant deformation is due to nearby slabs (Kula, Izanagi, Farallon) being strongly coupled to the plate through slab suction. The flow cell set-up by the Izanagi slab is dominant in controlling Pacific Plate kinematics at this time, because the trench-perpendicular length of the Izangai plate is relatively small (Morra et al., 2012). Induced flow in the model results in minimal surface uplift, so radial stress is not apparent. Instead, deformation is caused by induced flow, dragging sections of the plate with spatially varying tractions. As a result, deformation due to induced upwellings is minimally constrained. Smooth, homogenous style of coherent deformation is generally observed at the borders of divergent and passive margins in the models partly due to convection cells acting on the intervening space between plate boundaries (Butterworth et al., 2012).

There was a major tectonic plate reorganisation between 53–50 Ma (Whittaker et al., 2007; Cande and Stegman, 2011). This abrupt direction change has been linked to the subduction of the Pacific-Izanagi ridge (Whittaker et al., 2007). This tectonic reconfiguration is captured between the 62 and 52 Ma models. Between these times there

SED
6, 145–190, 2014

is a significant increase in deformation across the entire Pacific Plate (Figs. 2 and 3). By 52 Ma the Pacific-Izanagi ridge is fully subducted and the volume of slab material controlling the pull force on the Pacific is at the maximum of all the epochs modelled. The model velocities capture a significant change in absolute plate motion during this time interval. The 52 Ma model reflects a peak amplitude in total lithospheric deformation over the Plate compared to the other modelled times. However, we do not see a marked increase in volcanic flux at this time (Hillier, 2007; Clouard and Bonneville, 2005). This is in contrast to an expected increase in volcanism during such a period of rapid plate motion change (Anderson, 1994; Hieronymus and Bercovici, 2000).

Between 52 and 47 Ma the Junction Plate in the western Pacific has fully subducted leaving a smoother plate boundary between the Pacific and Philippine Plates. In this time period the amount of total global slab material directly pulling the Pacific Plate has reduced from ∼ 24 % to ∼ 15 %. Changing motions in the Pacific during the Cenozoic have previously been shown to be driven by the variations in slab-pull (Faccenna et al., 2012) and slab-suction (Conrad and Lithgow-Bertelloni, 2004). And, asymmetric distribution of slab material along the subduction zones partially controls the location of intraplate deformation (Clouard and Gerbault, 2008a).

The plate topology, subduction zone, and slab material configurations driving the 47 and 42 Ma models are relatively similar. In turn, the patterns of deformation across the Pacific Plate are similar.

4.3 Plate deformation correlated with magmatic events and evidence for non-plume related intraplate volcanism

A variety of age-dated volcanic structures formed across the Pacific Plate between 72 and 42 Ma (Fig. 7), which can be compared with the deformation predicted by our models. The complexity and abundance of seafloor features are highlighted by the use of the vertical gravity gradient in Fig. 7, however seafloor structures that have been sampled and dated to this time period are scarce (Hillier, 2007). Plate deformation does not necessarily generate volcanism, just as volcanism can take place without plate defor-

SED
6, 145–190, 2014

mation, e.g. small-scale convection that is not directly related to deformation. Although plate deformation may induce upwelling and decompression melting, the plate deformation (cracking) can also serve to simply facilitate the rise of melts that already exist or are produced by other mechanisms.

The northernmost area of Pacific intraplate volcanism in Fig. 7 are the Emperor Seamounts (Duncan and Keller, 2004), a product of plume-plate interaction (Sharp and Clague, 2006). However, throughout its formation history, subduction driven plate deformation is seen to overlap with the chain. A region of high-strain, between 15–30° N, encompasses the southern part of the Emperor chain in the 52 Ma model run (Fig. 3). Rather than produce new volcanism, deformation induced during the 52 Ma time period may impose small stress-bends in the pre-existing linear chain (Koppers and Staudigel, 2005). The 47 Ma model (Fig. 4) continues to show plate-strain, with a diminished magnitude, overlapping with the Hawaiian-Emperor chain. Volcanism is active during the 42 Ma model time period in Hawaii (Sharp and Clague, 2006) and the chain continues to show age-progressive volcanism after the bend at 47 Ma. But the 42 Ma model shows minimal plate deformation correlated with the location of the chain.

In the north-east of the Pacific Plate lies the Musicians Volcanic Ridges, that have active volcanism coeval with our model run epochs, between 72 and 42 Ma. This may be considered late-stage volcanism occurring after the initial formation from a hotspot interacting with a spreading ridge from 96 to 75 Ma (Pringle, 1993; Kopp et al., 2003). In the 62 and 52 Ma models in the Musicians seamounts there is increased deformation indicated by the model (Fig. 3). The 47 and 42 Ma models continue to show deformation around the Musicians ridge.

The Louisville seamount chain in the South Pacific documents a history of volcanism from 82 to 42 Ma (Koppers et al., 2010, 2011), associated with classical hotspot activity (Koppers et al., 2004). There is plate deformation toward the north of the chain in the 42 Ma model (Fig. 5).

The Austral seamounts show volcanism between 62 and 52 Ma (Clouard and Bonneville, 2005). This region of seamounts is influenced by many hotspots (Clouard and

SED
6, 145–190, 2014

Bonneville, 2005) and also shows correlation with highly deformed lithosphere at 52 Ma (Fig. 3). This suggests correlation between hotspots located under lithosphere weakened by previous volcanism (Hillier, 2007).

In the western Pacific (Fig. 7) there are several clusters of seamounts that together encompass the Western Pacific Seamount Province. This province shows weak age-progression in some areas (Ito and van Keken, 2007), suggesting some formation mechanism other than a plume. Koppers et al. (2003) show that there are in fact some age progressions in this region, but overall is a rather complex area with a spike in volcanism lasting until ~ 70 Ma. This province includes the Japanese Seamounts (Ozima et al., 1983) in the north, the Mid-Pacific Mountains (Pringle, 1993) that show weak age progression in the central region, and the Magellan seamounts to the south. Between 82 and 62 Ma there are only four Japanese seamounts displaying volcanism, with no mapped features correlating with our modelled plate-strain.

The Line Islands in the central Pacific are considered to have formed through volcanism due to lithospheric extension (Davis et al., 2002). Their temporal appearance between 80 and 68 Ma is not correlated with subduction driven deformation observed in the 62 Ma model. The Line Islands show reduced volcanism after this time until 55 Ma without any deforming regions coinciding with their formation.

The initial formation of the Gilbert Ridge can be extended back in time along the Marshall Islands to around 100 Ma (Konter et al., 2008; Koppers et al., 2003). Basement near the ridge was likely preconditioned to volcanism (Koppers et al., 2007) because of the emplacement of volcanic sills during the formation of the Ontong-Java and Hikurangi Plateaus around 125 Ma. The location of the Gilbert chain follows a likely zone of weakness extending north from the Manahiki-Chizca ridge, and running parallel to existing fracture zones (Fig. 2). The Gilbert ridge has been shown to have poor age progression and also shows signs of stress bends at times after formation (Koppers et al., 2007). Volcanism is expressed from 72 to 62 Ma at the Gilbert ridge and later at the Tuvalu-Ellice and Samoan seamount chain (Koppers and Staudigel, 2005). This chain trends and extends in the same north-west direction as the zone of high-strain banding

SED
6, 145–190, 2014

in the central Pacific seen in Fig. 2. It has been shown that seamount chains are generally aligned with the direction of the most tensile principal tectonic stress (Hieronymus and Bercovici, 2000). The modelled Pacific Plate is experiencing tensional deformation along a zone aligned with the orientation of this feature (Fig. 2). The timing of the modelled lithospheric deformation correlates with the formation age of 67 Ma (Koppers and Staudigel, 2005), with continued stress likely influencing a long slow stress-bend after the Gilbert chain's formation. Deformation of the Pacific lithosphere overprinting pre-existing weaknesses seems to have been significant enough to activate the Gilbert chain around this time. Melt material may have already existed in the upper-mantle from the events around 100 Ma, only requiring the changing tectonic stresses, incited by the subducting Izangi slab, to initiate surface volcanism.

The Tokelau seamounts and Phoenix Islands are formed between 72 and 62 Ma in the eastern Pacific (Koppers and Staudigel, 2005), away from any significant tectonic deformation. The Tokelau seamounts are volcanically active between the 62 and 47 Ma models, correlating with a well-defined region of high-strain (Figs. 3–5). Formation of these structures are likely influenced by lithospheric extension (Koppers and Staudigel, 2005) on crust weakened by nearby fracture zones.

The Tarava seamounts become active for the 42 Ma model and are thought to have formed from a hotspot influenced by lithospheric stress (Clouard et al., 2003). This is consistent with the regional deformed area overlapping the location of the reconstructed sample location (Fig. 5). An unknown source mechanism has produced volcanic activity along the poorly sampled and dated nearby Tuamotus seamounts, around 40–50 Ma, visible in the the 47 Ma and 42 Ma models (Figs. 4 and 5). There is minimal correlation between modelled plate deformation and the formation of these seamounts.

It has previously been shown that present day subduction zone forces on the Pacific Plate lead to internal deformation (Clouard and Gerbault, 2008a, b). Extensional mechanisms and lithospheric thickness variations can contribute to enhanced volcanism on ridges and hotspots, but neither mechanism is likely the sole source of seamount chains (Pilger, 2008). Lithospheric weaknesses (e.g. fracture zones, pre-existing mag-

SED
6, 145–190, 2014

matism) that override a source of melt material, possibly derived from mantle plumes too weak to penetrate the surface, may be perturbed by tectonic stresses due to plate motion changes, inturn exciting surface eruption. Age-dated Late Cretaceous and early Cenozoic seafloor structures across the Pacific show signs of Pacific-wide plate deformation. Intraplate volcanism sampled across the Pacific is partially indicative of a proposed global reorganisation (Whittaker et al., 2007; Cande and Stegman, 2011) between about 62 and 47 Ma and may be considered as a proxy for stress on the plate (Clouard and Gerbault, 2008a). Because the stress state of the lithosphere, plate deformation, and subsequent volcanism are inherently mixed, but are not necessarily mutually exclusive, it is difficult to extract a definitive location of volcanism based on stress or deformation alone, or vice-versa. This is even more so where there is pre-existing hotspot volcanism in reactivated seamount chains. However, deformation predicted by our models gives an indication of potential sites of intraplate volcanism that are related to anomalously stressed lithosphere.

4.4 Modelled lithospheric structure influencing plate deformation

There is competition between thermal contraction that strengthens the lithosphere during cooling as the lithosphere gets older and thicker (Koppers and Watts, 2010) and load-induced stress relaxation that weakens it. However, it is found that plate thickness seems to have no noticeable effect on plate deformation, driven by large-scale convection in our models, regardless of the tectonic configuration. This is likely because the plate rheology is homogenous and there is no heat flow in the model that would otherwise create a weakened crust (Shaw and Lin, 1996). Also the thickness variations are comparatively small to the major convective cells in the model domain.

The rheology of the modelled subducting plate and the mantle will influence the deformation of the plate. In the models, decreasing the lithosphere viscosity to $50 \times \eta_m$ or increasing it to $200 \times \eta_m$ will make the model evolve slower or faster, respectively. However, regions of deformation remain broadly consistent between models with a different viscosity lithosphere. Intraplate deformation resulting from the stresses imposed

SED
6, 145–190, 2014

by the subduction and mantle drag/suction forces are a robust prediction of the model. Whether the stresses are sufficient to cause intraplate deformation depends on the actual rheological parameters of the Pacific Plate. A subsequent increase in deformation may result in volcanism only if melt material is available, and the lithosphere has pre-existing lines of weakness and/or is weak enough to fracture (Ballmer et al., 2009; Hieronymus and Bercovici, 2000).

5 Conclusions

During the Late Cretaceous and early Cenozoic the Pacific Plate underwent a major tectonic shift in its primary driving forces. In our models prior to 52 Ma, the Pacific was controlled by the Izanagi, Kula, and Farallon subducting plates surrounding it, and to a lesser extent by a small subducting slab attached at the East Junction subduction zone. From 52 Ma onwards, following the subduction of the Pacific-Izanagi ridge, the Pacific Plate was primarily controlled by slab-pull in the north-west. The absolute motions of the Pacific derived from subduction driven forces correspond well with other modelled plate reconstructions (Seton et al., 2012; Chandler et al., 2012), when model assumptions and simplifications are taken into account. An overestimate of Pacific mantle plume motion constraints used in other absolute reference frames (Doubrovine et al., 2012; Wessel and Kroenke, 2008) is the likely reason for their inconsistencies with Pacific motion in our subduction driven model. The subsequent motion of the plate controls the deformation in the attached subducting plate. We find the regions of highest deformation occur directly adjacent to the most voluminous subducting slabs. Several areas of deformation across the Pacific can be linked to age-dated intraplate volcanism. The seamount chains of Hawaii-Emperor, Louisville, and Tokelau are subject to lithospheric deformation occurring the early Cenozoic. Plate-scale extensional stresses between our modelled time intervals correlate with a large section of the location and timing of formation of the Gilbert chain, suggesting an origin largely due to lithospheric extension at this time. The Musicians Volcanic Ridges, which likely formed

SED
6, 145–190, 2014

by traditional plume mechanisms, spatially correlate with modelled lithospheric stress and is a likely candidate for late-stage volcanism between 52 and 42 Ma. Our simplified 3-D subduction simulations suggest stress-induced deformation in the Pacific during the Late Cretaceous and early Cenozoic is partially controlled by plate-scale kinematics. Our dynamic models, combined with kinematically reconstructed absolute plates motions, confirm the view that the Hawaiian-Emperor bend does not reflect a change in absolute plate motion, but that it reflects the slowdown of the Hawaiian plume drift.

Appendix A

Comparison of initial model condition with Slab1.0

We use 10 Myr of subduction history to build the slabs attached to the geodynamic model subducting plates. The kinematics of the plate model (Seton et al., 2012) determines the total volume of material, dip, and depth of the slab. We find these dips to be comparable to the available Slab1.0 (Hayes et al., 2012) present day slabs (Figs. A1–A6).

Appendix B

Volume of subducted material

Plate convergent velocities are determined for each point along the reconstructed subduction zone for each time period. Oceanic lithosphere thickness is derived from the paleo-reconstruction model (Seton et al., 2012) along with sampling age grids with a $1^{\circ} \times 1^{\circ}$ resolution (Müller et al., 2013). Using a Half-Space Cooling model truncated at 95 km (after Chapter 4.2 Schubert et al., 2001) the thickness of the lithosphere, z, is

SED
6, 145–190, 2014

determined as

$$z = \mathrm{erf}^{-1}\left(\frac{T_\mathrm{l} - T_\mathrm{o}}{T_\mathrm{m} - T_\mathrm{o}}\right) 2\sqrt{\kappa}\sqrt{\mathrm{age}}, \quad \text{(B1)}$$

where, erf^{-1} is the inverse of the error function, $T_\mathrm{l} = 1300\,^{\circ}\mathrm{C}$ and is the isotherm of the lithosphere, $T_\mathrm{o} = 0\,^{\circ}\mathrm{C}$ and is the surface temperature, $T_\mathrm{m} = 1600\,^{\circ}\mathrm{C}$ and is the temperature of the mantle, $\kappa = 8 \times 10^{-8}\,\mathrm{m\,s^{-1}}$ and is the thermal diffusivity constant, and age is the age of the lithosphere sampled from the age grids. We calculate the volume of the slab as the convergence rate times the lithospheric thickness times each subduction segment length (from the resolution of the plate model). Figures B1–B4 show the amount of globally subducted material for each of the model time periods.

Acknowledgements. Thanks to C. Heine and S. Williams for fruitful discussions.

References

Anderson, D.: Superplumes or supercontinents?, Geology, 22, 39–42, doi:10.1130/0091-7613(1994)022<0039:SOS>2.3.CO;2, 1994. 148, 158

Ballmer, M., van Hunen, J., Ito, G., Bianco, T., and Tackley, P.: Intraplate volcanism with complex age-distance patterns: a case for small-scale sublithospheric convection, Geochem. Geophy. Geosy., 10, Q06015, doi:10.1029/2009GC002386, 2009. 147, 163

Ballmer, M. D., Conrad, C. P., Smith, E. I., and Harmon, N.: Non-hotspot volcano chains produced by migration of shear-driven upwelling toward the East Pacific Rise, Geology, 41, 479–482, doi:10.1130/G33804.1, 2013. 147

Billen, M.: Modeling the dynamics of subducting slabs, Annu. Rev. Earth Pl. Sc., 36, 325–56, doi:10.1146/annurev.earth.36.031207.124129, 2008. 149

Bonatti, E.: Not so hot "hot spots" in the oceanic mantle, Science, 250, 107–111, doi:10.1126/science.250.4977.107, 1990. 147

Boresi, A. P. and Schmidt, R. J.: Advanced Mechanics of Materials, John Wiley and Sons, 2003. 151

SED
6, 145–190, 2014

Boyden, J., Müller, R., Gurnis, M., Torsvik, T., Clark, J., Turner, M., Ivey-Law, H., Watson, R., and Cannon, J.: Next-generation plate-tectonic reconstructions using GPlates, in: Geoinformatics: Cyberinfrastructure for the Solid Earth Sciences, edited by: Keller, G. R. and Baru, C., Chap. 7, Cambridge University Press, 95–116, doi:10.1017/CBO9780511976308.008, 2011. 149

Butterworth, N., Quevedo, L., Morra, G., and Müller, R.: Influence of overriding plate geometry and rheology on subduction, Geochem. Geophy. Geosy., 13, Q06W15, doi:10.1029/2011GC003968, 2012. 148, 150, 151, 152, 157, 175

Cande, S. C. and Stegman, D. R.: Indian and African plate motions driven by the push force of the Réunion plume head, Nature, 475, 47–52, doi:10.1038/nature10174, 2011. 148, 157, 162

Capitanio, F., Stegman, D., Moresi, L., and Sharples, W.: Upper plate controls on deep subduction, trench migrations and deformations at convergent margins, Tectonophysics, 483, 80–92, doi:10.1016/j.tecto.2009.08.020, 2010. 150

Chandler, M. T., Wessel, P., Taylor, B., Seton, M., Kim, S.-S., and Hyeong, K.: Reconstructing Ontong Java Nui: implications for Pacific absolute plate motion, hotspot drift and true polar wander, Earth Planet. Sc. Lett., 331–332, 140–151, doi:10.1016/j.epsl.2012.03.017, 2012. 148, 156, 163

Clouard, V. and Bonneville, A.: Ages of seamounts, islands, and plateaus on the Pacific plate, Geol. Soc. Am. S., 388, 71–90, doi:10.1130/0-8137-2388-4.71, 2005. 148, 158, 159

Clouard, V. and Gerbault, M.: Break-up spots: Could the Pacific open as a consequence of plate kinematics?, Earth Planet. Sc. Lett., 265, 195–208, doi:10.1016/j.epsl.2007.10.013, 2008a. 148, 151, 158, 161, 162

Clouard, V. and Gerbault, M.: Reply to "Break-up spots: Could the Pacific open as a consequence of plate kinematics?" Comment by R. Pilger, Earth Planet. Sc. Lett., 275, 196–199, doi:10.1016/j.epsl.2008.08.008, 2008b. 161

Clouard, V., Bonneville, A., and Gillot, P.-Y.: The Tarava Seamounts: a newly characterized hotspot chain on the South Pacific Superswell, Earth Planet. Sc. Lett., 207, 117–130, doi:10.1016/S0012-821X(02)01143-3, 2003. 161

Conrad, C. and Lithgow-Bertelloni, C.: How mantle slabs drive plate tectonics, Science, 298, 207, doi:10.1126/science.1074161, 2002. 148

SED
6, 145–190, 2014

Conrad, C. and Lithgow-Bertelloni, C.: The temporal evolution of plate driving forces: importance of "slab suction" versus "slab pull" during the Cenozoic, J. Geophys. Res., 109, B10407, doi:10.1029/2004JB002991, 2004. 148, 158

Conrad, C. P., Bianco, T. A., Smith, E. I., and Wessel, P.: Patterns of intraplate volcanism controlled by asthenospheric shear, Nat. Geosci., 4, 317–321, doi:10.1038/ngeo1111, 2011. 147

Courtillot, V., Davaille, A., Besse, J., and Stock, J.: Three distinct types of hotspots in the Earth's mantle, Earth Planet. Sc. Lett., 205, 295–308, doi:10.1016/S0012-821X(02)01048-8, 2003. 147

Davis, A. S., Gray, L. B., Clague, D. A., and Hein, J. R.: The Line Islands revisited: new $^{40}Ar/^{39}Ar$ geochronologic evidence for episodes of volcanism due to lithospheric extension, Geochem. Geophy. Geosy., 3, 1018, doi:10.1029/2001GC000190, 2002. 147, 151, 160

Doubrovine, P., Steinberger, B., and Torsvik, T.: Absolute plate motions in a reference frame defined by moving hot spots in the Pacific, Atlantic, and Indian oceans, J. Geophys. Res., 117, B09101, doi:10.1029/2011JB009072, 2012. 148, 152, 153, 154, 155, 156, 163, 175

Duncan, R. A. and Keller, R. A.: Radiometric ages for basement rocks from the Emperor Seamounts, ODP Leg 197, Geochem. Geophy. Geosy., 5, Q08L03, doi:10.1029/2004GC000704, 2004. 159

Faccenna, C., Becker, T. W., Lallemand, S., and Steinberger, B.: On the role of slab pull in the Cenozoic motion of the Pacific plate, Geophys. Res. Lett., 39, L03305, doi:10.1029/2011GL050155, 2012. 148, 158

Gueydan, F., Morency, C., and Brun, J.-P.: Continental rifting as a function of lithosphere mantle strength, Tectonophysics, 460, 83–93, doi:10.1016/j.tecto.2008.08.012, 2008. 151

Hayes, G. P., Wald, D. J., and Johnson, R. L.: Slab1.0: a three-dimensional model of global subduction zone geometries, J. Geophys. Res.-Sol. Ea., 117, B01302, doi:10.1029/2011JB008524, 2012. 149, 164, 181, 182, 183, 184, 185, 186

Hieronymus, C. and Bercovici, D.: Non-hotspot formation of volcanic chains: control of tectonic and flexural stresses on magma transport, Earth Planet. Sc. Lett., 181, 539–554, doi:10.1016/S0012-821X(00)00227-2, 2000. 147, 148, 158, 161, 163

Hillier, J.: Pacific seamount volcanism in space and time, Geophys. J. Int., 168, 877–889, doi:10.1111/j.1365-246X.2006.03250.x, 2007. 148, 158, 160

SED
6, 145–190, 2014

Hirano, N., Takahashi, E., Yamamoto, J., Abe, N., Ingle, S. P., Kaneoka, I., Hirata, T., Kimura, J.-I., Ishii, T., Ogawa, Y., Machida, S., and Suyehiro, K.: Volcanism in response to plate flexure, Science, 213, 1426–1428, doi:10.1126/science.1128235, 2006. 147

Ito, G. and van Keken, P. E.: Hotspots and melting anomalies, in: Treatise on Geophysics, edited by: Bercovici, D., vol. 7, Mantle Dynamics, Elsevier, 371–435, 2007. 147, 160

Konter, J. G., Hanan, B. B., Blichert-Toft, J., Koppers, A. A. P., Plank, T., and Staudigel, H.: One hundred million years of mantle geochemical history suggest the retiring of mantle plumes is premature, Earth Planet. Sc. Lett., 275, 285–295, doi:10.1016/j.epsl.2008.08.023, 2008. 160

Kopp, H., Kopp, C., Morgan, J. P., Flueh, E. R., Weinrebe, W., and Morgan, W.: Fossil hot spot-ridge interaction in the Musicians Seamount Province: geophysical investigations of hot spot volcanism at volcanic elongated ridges, J. Geophys. Res., 108, 2160, doi:10.1029/2002JB002015, 2003. 159

Koppers, A. A. P.: Mantle plumes persevere, Nat. Geosci., 4, 816–817, doi:10.1038/ngeo1334, 2011. 147

Koppers, A. and Staudigel, H.: Asynchronous bends in Pacific seamount trails: a case for extensional volcanism?, Science, 307, 904–907, doi:10.1126/science.1107260, 2005.159, 160, 161

Koppers, A. A. P. and Watts, A. B.: Intraplate seamounts as a window into deep Earth processes, Oceanography, 23, 42–57, doi:10.5670/oceanog.2010.61, 2010. 162

Koppers, A. A. P., Staudigel, H., Pringle, M., and Wijbrans, J.: Short-lived and discontinuous intraplate volcanism in the South Pacific: hot spots or extensional volcanism?, Geochem. Geophy. Geosy., 4, 1089, doi:10.1029/2003GC000533, 2003. 147, 160

Koppers, A. A. P., Duncan, R., and Steinberger, B.: Implications of a nonlinear $^{40}Ar/^{39}Ar$ age progression along the Louisville seamount trail for models of fixed and moving hot spots, Geochem. Geophy. Geosy., 5, Q06L02, doi:10.1029/2003GC000671, 2004. 159

Koppers, A. A. P., Staudigel, H., Morgan, J. P., and Duncan, R.: Nonlinear $^{40}Ar/^{39}Ar$ age systematics along the Gilbert Ridge and Tokelau Seamount Trail and the timing of the Hawaii-Emperor Bend, Geochem. Geophy. Geosy., 8, Q06L13, doi:10.1029/2006GC001489, 2007. 160

Koppers, A. A. P., Yamazaki, T., and Geldmacher, J.: Louisville Seamount Trail: implications for geodynamic mantle flow models and the geochemical evolution of primary hotspots, IODP Scientific Prospectus, 330, doi:10.2204/iodp.sp.330.2010, 2010. 159

SED
6, 145–190, 2014

Koppers, A. A. P., Gowen, M. D., Colwell, L. E., Gee, J. S., Lonsdale, P. F., Mahoney, J. J., and Duncan, R.: New $^{40}Ar/^{39}Ar$ age progression for the Louisville hot spot trail and implications for inter–hot spot motion, Geochem. Geophy. Geosy., 12, Q0AM02, doi:10.1029/2011GC003804, 2011. 159

Lee, C.-T. A. and Grand, S. P.: Intraplate volcanism, Nature, 482, 314–315, doi:10.1038/482314a, 2012. 147

Li, Z.-H. and Ribe, N. M.: Dynamics of free subduction from 3-D boundary element modeling, J. Geophys. Res., 117, B06408, doi:10.1029/2012JB009165, 2012. 150

Lithgow-Bertelloni, C. and Richards, M.: The dynamics of Cenozoic and Mesozoic plate motions, Rev. Geophys., 36, 27–78, doi:10.1029/97RG02282, 1998. 151

Liu, L. and Stegman, D. R.: Origin of Columbia River flood basalt controlled by propagating rupture of the Farallon slab, Nature, 482, 386–390, doi:10.1038/nature10749, 2012. 147

Matthews, K., Müller, R., Wessel, P., and Whittaker, J.: The tectonic fabric of the ocean basins, J. Geophys. Res., 116, B12109, doi:10.1029/2011JB008413, 2011. 175

Morgan, W.: Convection plumes in the lower mantle, Nature, 230, doi:10.1038/230042a0, 1971. 147

Morra, G., Chatelain, P., Tackley, P., and Koumoutsakos, P.: Large scale three-dimensional boundary element simulation of subduction, in: Computational Science – ICCS 2007, edited by: Shi, Y., Albada, G., Dongarra, J., and Sloot, P., Lecture Notes in Computer Science, Vol. 4489, 1122–1129, Springer, Berlin, Heidelberg, 1122–1129, doi:10.1007/978-3-540-72588-6_178, 2007. 148, 150

Morra, G., Quevedo, L., and Muller, R. D.: Spherical dynamic models of top-down tectonics, Geochem. Geophy. Geosy., 13, 1–66, doi:10.1029/2011GC003843, 2012. 148, 149, 150, 152, 155, 157

Morra, G., Seton, M., Quevedo, L., and Müller, R. D.: Organization of the tectonic plates in the last 200 Myr, Earth Planet. Sc. Lett., 373, 93–101, doi:10.1016/j.epsl.2013.04.020, 2013. 148

Müller, R., Dutkiewicz, A., Seton, M., and Gaina, C.: Seawater chemistry driven by supercontinent assembly, breakup, and dispersal, Geology, 41, 907–910, doi:10.1130/G34405.1, 2013. 149

O'Neill, C., Müller, D., and Steinberger, B.: On the uncertainties in hot spot reconstructions and the significance of moving hot spot reference frames, Geochem. Geophy. Geosy., 6, Q04003, doi:10.1029/2004GC000784, 2005. 155, 156

SED
6, 145–190, 2014

Ozima, M., Kaneoka, I., Saito, K., Honda, M., Yanagisawa, M., and Takigami, Y.: Summary of geochronological studies of submarine rocks from the western Pacific Ocean, in: Geodynamics of the Western Pacific-Indonesian Region, edited by: Hilde, T. W. C., and Uyeda, S., AGU, vol. 11, 137–142 doi:10.1029/GD011p0137, 1983. 160

Pilger, R.: Discussion of "Break-up spots: could the Pacific open as a consequence of plate kinematics?" by Clouard and Gerbault, Earth Planet. Sc. Lett., 275, 193–195, doi:10.1016/j.epsl.2008.08.005, 2008. 161

Pringle, M. S.: Age progressive volcanism in the Musicians seamounts: a test of the hot spot hypothesis for the late Cretaceous Pacific, in: The Mesozoic Pacific: Geology, Tectonics, and Volcanism: A Volume in Memory of Sy Schlanger, Geophys. Monogr. Ser, AGU, Washington, D.C., vol. 77, 187–216, doi:10.1029/GM077p0187, 1993. 159, 160

Quevedo, L., Hansra, B., Morra, G., Butterworth, N., and Müller, R. D.: Oblique mid ocean ridge subduction modelling with the parallel fast multipole boundary element method, Comput. Mech., 51, 455–463, doi:10.1007/s00466-012-0751-5, 2012a. 148

Quevedo, L., Morra, G., and Müller, R. D.: Global paleo-lithospheric models for geodynamical analysis of plate reconstructions, Phys. Earth Planet. In., 212–213, 106–113, doi:10.1016/j.pepi.2012.09.007, 2012b. 149

Ribe, N. M.: Bending mechanics and mode selection in free subduction: a thin-sheet analysis, Geophys. J. Int., 180, 559–576, doi:10.1111/j.1365-246X.2009.04460.x, 2010. 150

Ricard, Y., Richards, M., Lithgow-Bertelloni, C., and Le Stunff, Y.: A geodynamic model of mantle density heterogeneity, J. Geophys. Res.-Sol. Ea., 98, 21895–21909, doi:10.1029/93JB02216, 1993. 155

Romanowicz, B. and Gung, Y.: Superplumes from the core-mantle boundary to the lithosphere: implications for heat flux, Science, 296, 513–516, doi:10.1126/science.1069404, 2002. 147

Sandwell, D. and Fialko, Y.: Warping and cracking of the Pacific plate Warping and cracking of the Pacific plate by thermal contraction, J. Geophys. Res., 109, B10411, doi:10.1029/2004JB003091, 2004. 147

Sandwell, D. and Smith, W. H. F.: Global marine gravity from retracked Geosat and ERS-1 altimetry: ridge segmentation versus spreading rate, J. Geophys. Res., 114, B01411, doi:10.1029/2008JB006008, 2009. 180

Sandwell, D., Winterer, E., Mammerickx, J., Duncan, R., Lynch, M., Levitt, D., and Johnson, C.: Evidence for diffuse exension of the Pacific plate from Pukapuka ridges and cross-grain gravity lineations, J. Geophys. Res., 100, 15087–15099, doi:10.1029/95JB00156, 1995. 147

SED
6, 145–190, 2014

Schellart, W.: Quantifying the net slab pull force as a driving mechanism for plate tectonics, Geophys. Res. Lett., 31, L07611, doi:10.1029/2004GL019528, 2004. 149
Schubert, G., Turcotte, D. L., and Olson, P.: Mantle Convection in the Earth and Planets, Cambridge University Press, 2001. 164
Seton, M. and Müller, R.: Reconstructing the junction between Panthalassa and Tethys since the Early Cretaceous, Eastern Australian Basins III. Petroleum Exploration Society of Australia. Special Publication, 263–266, 2008. 152
Seton, M., Müller, R., Zahirovic, S., Gaina, C., Torsvik, T., Shephard, G., Talsma, A., Gurnis, M., Turner, M., Maus, S., and Chandler, M.: Global continental and ocean basin reconstructions since 200 Ma, Earth-Sci. Rev., 113, 212–270, doi:10.1016/j.earscirev.2012.03.002, 2012. 148, 149, 152, 153, 154, 155, 156, 163, 164, 175, 179
Sharp, W. and Clague, D.: 50-Ma initiation of Hawaiian-Emperor bend records major change in Pacific plate motion, Science, 313, 1281, doi:10.1126/science.1128489, 2006. 155, 159
Shaw, W. J. and Lin, J.: Models of ocean ridge lithospheric deformation: dependence on crustal thickness, spreading rate, and segmentation, J. Geophys. Res., 101, 17977–17993, doi:10.1029/96JB00949, 1996. 162
Staudigel, H., Park, K.-H., Pringle, M., Rubenstone, J., Smith, W., and Zindler, A.: The longevity of the South Pacific isotopic and thermal anomaly, Earth Planet. Sc. Lett., 102, 24–44, doi:10.1016/0012-821X(91)90015-A, 1991. 148
Stegman, D., Farrington, R., Capitanio, F., and Schellart, W.: A regime diagram for subduction styles from 3-D numerical models of free subduction, Tectonophysics, 483, 29–45, doi:10.1016/j.tecto.2009.08.041, 2010. 150
Tarduno, J., Bunge, H.-P., Sleep, N., and Hansen, U.: The Bent Hawaiian-Emperor hotspot track: inheriting the mantle wind, Science, 324, 50–53, doi:10.1126/science.1161256, 2009. 155, 157
Tarduno, J. A.: On the motion of Hawaii and other mantle plumes, Chem. Geol., 241, 234—247, doi:10.1016/j.chemgeo.2007.01.021, the Great Plume Debate: Testing the Plume Theory, 2007. 157
Wessel, P. and Kroenke, L. W.: Pacific absolute plate motion since 145 Ma: an assessment of the fixed hot spot hypothesis, J. Geophys. Res., 113, B06101, doi:10.1029/2007JB005499, 2008. 148, 156, 163, 179

SED
6, 145–190, 2014

Whittaker, J. M., Muller, R. D., Leitchenkov, G., Stagg, H., Sdrolias, M., Gaina, C., and Goncharov, A.: Major Australian-Antarctic plate reorganization at Hawaiian-Emperor Bend Time, Science, 318, 83–86, doi:10.1126/science.1143769, 2007. 148, 157, 162

Wilson, J.: A possible origin of the Hawaiian Islands, Can. J. Phys., 41, 863–870, doi:10.1139/p63-094, 1963. 147

SED

6, 145–190, 2014

Table 1. Reference model parameters.

Parameter	Symbol	Non-dimensional value	Natural value	Units
Earth Radius	r_E	1	6371	km
Mantle Viscosity	η_m	1	10^{21}	Pas
Mantle Density	ρ_m	50	3300	kgm^{-3}
Slab Viscosity	η_s	$100 \times \eta_m$	$100 \times \eta_m$	Pas
Slab Density	ρ_s	80	3330	kgm^{-3}

SED
6, 145–190, 2014

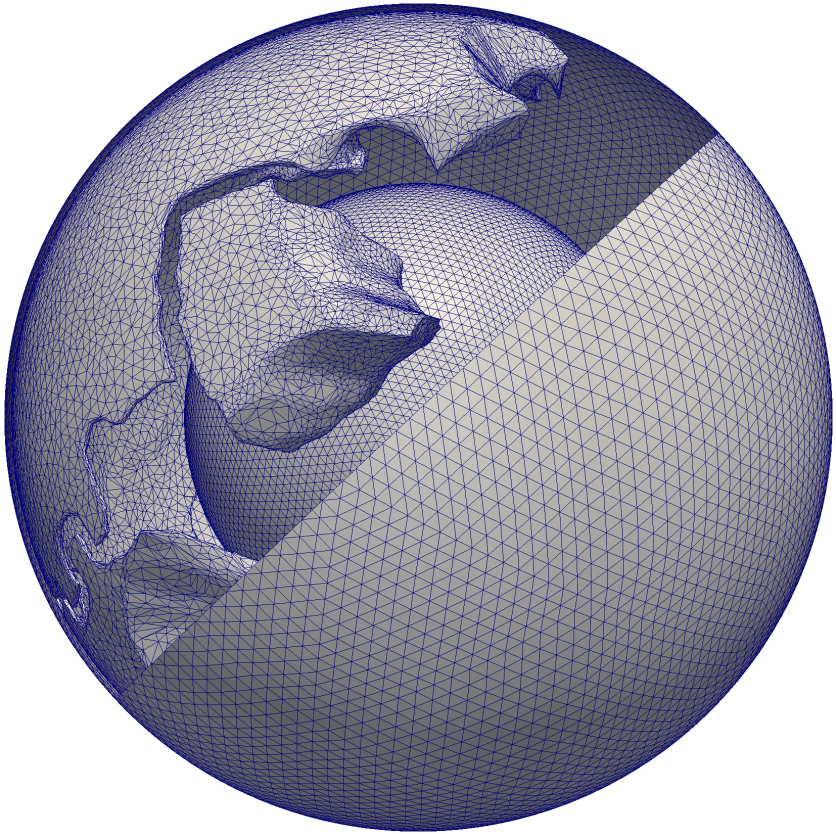

Fig. 1. The initial starting model used for input into BEM-Earth. Each isosurface bounds a region of discrete viscosity and density as described in Table 1. The external Earth surface has been peeled back to show the other core and plate isosurfaces. The modelled plates, here at 42 Ma, are the Kula, Farallon, and Pacific. The blue mesh is indicative of model resolution and shows the panels that are free to deform.

SED
6, 145–190, 2014

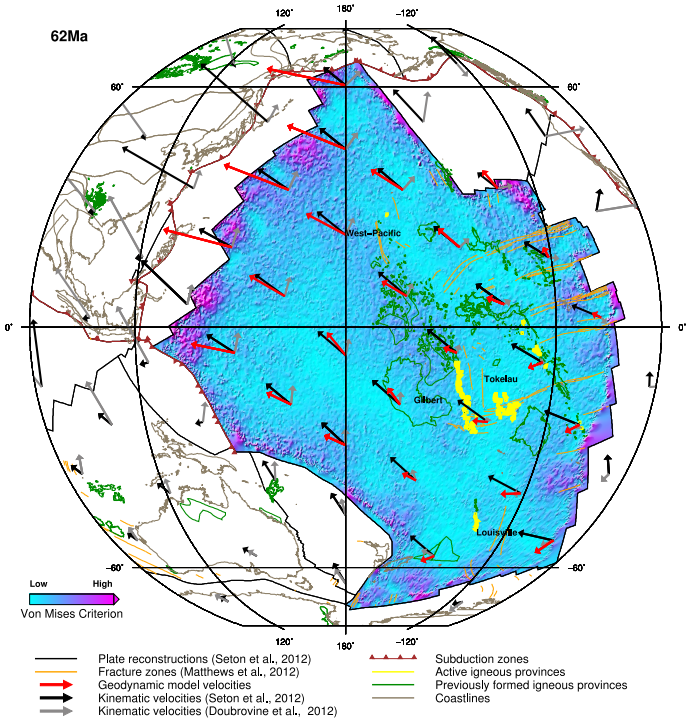

Fig. 2. Pacific Plate reconstruction at 62 Ma. Paleo-plate reconstructed positions (Seton et al., 2012) are outlined in black, with attached subduction zones in red. Velocities of kinematic plate reconstruction models are shown by the black (Seton et al., 2012) and grey arrows (Doubrovine et al., 2012). Our subduction model derived velocity vectors are shown by red arrows. The yellow features are the reconstructed positions of age-dated igneous provinces that have appeared in the 10 Myr preceding the model (see discussion for references). Existing igneous structures are outlined in green. Significant locations are labelled. Orange lines are the reconstructed fracture zone locations (Matthews et al., 2011). The brown outlines represent the reconstructed positions of the present day coastlines. The aqua to magenta colour scale represents the non-dimensional von Mises Criterion of our model, with aqua representing minimal plate deformation and magenta representing the maximal deformation. Numbers on the colour scale are derived from non-dimensional model displacements. The smooth, homogenous style of deformation is at the borders of divergent and passive margins is likely due to convection cells acting in the intervening space between plates (Butterworth et al., 2012).

SED
6, 145–190, 2014

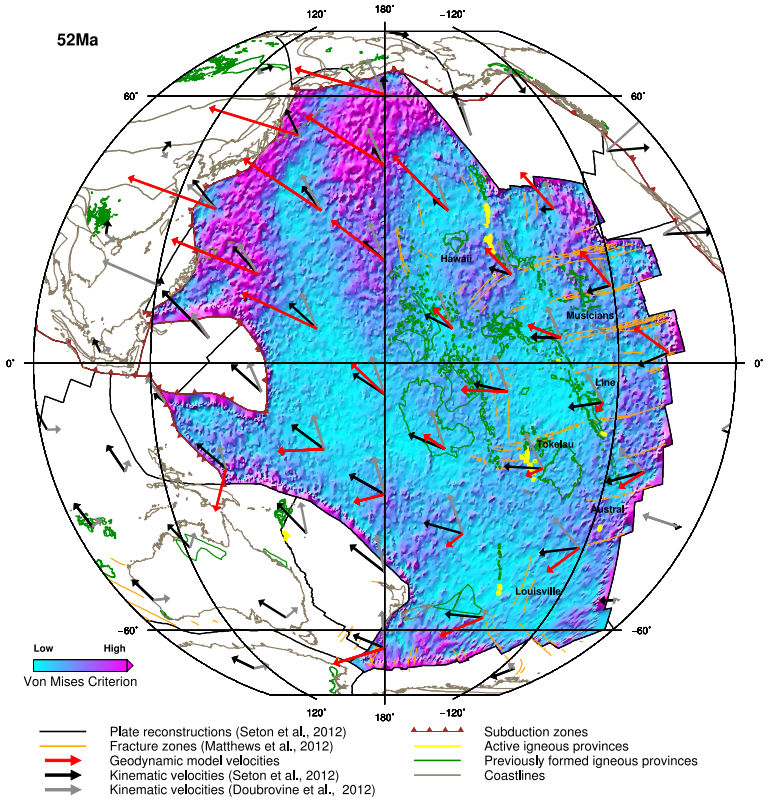

Fig. 3. Same as Fig. 2 but for the Pacific Plate reconstruction at 52 Ma.

SED
6, 145–190, 2014

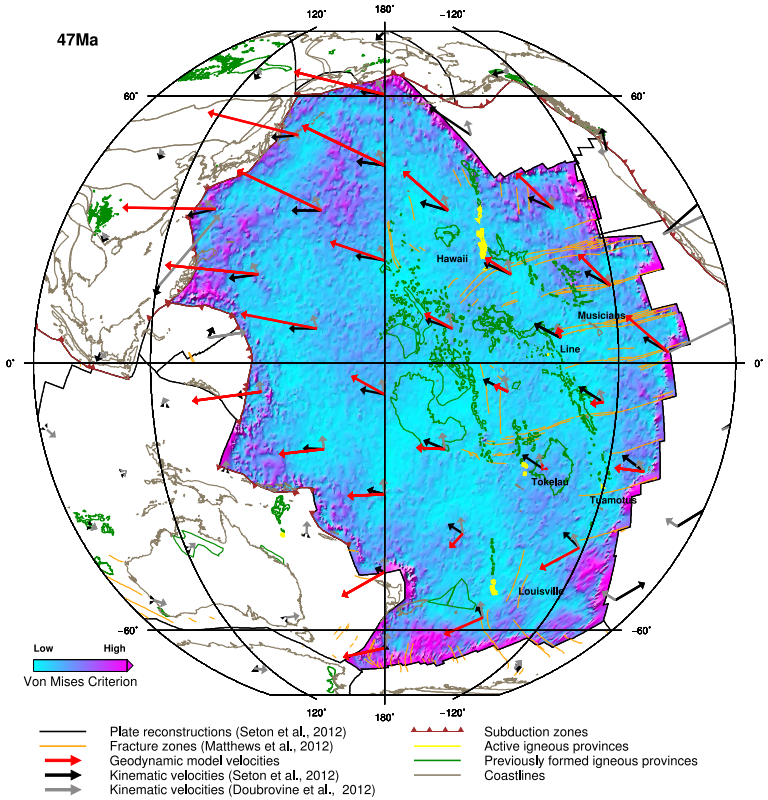

Fig. 4. Same as Fig. 2 but for the Pacific Plate reconstruction at 47 Ma.

SED
6, 145–190, 2014

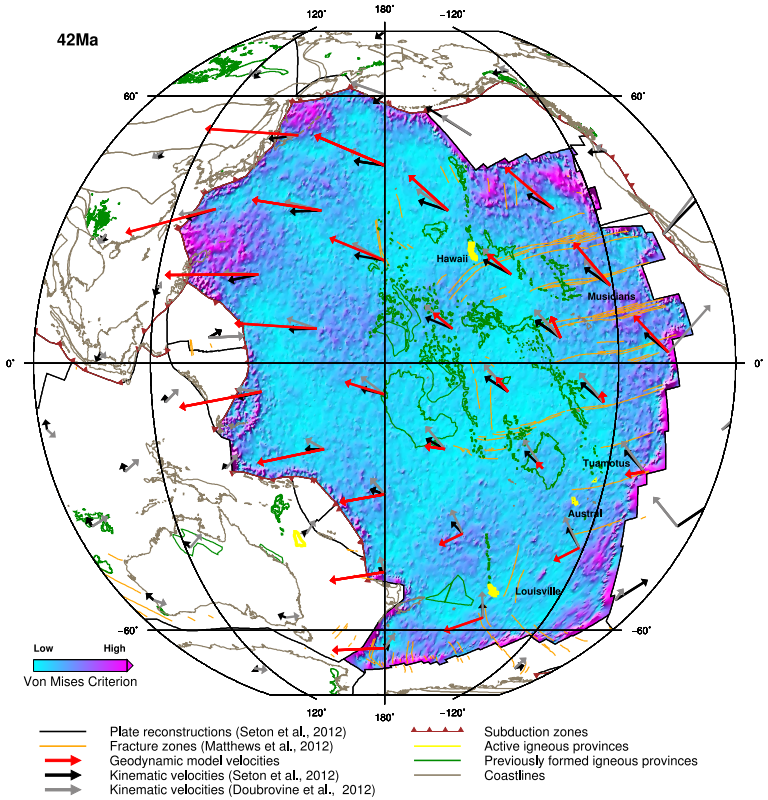

Fig. 5. Same as Fig. 2 but for the Pacific Plate reconstruction at 42 Ma.

SED
6, 145–190, 2014

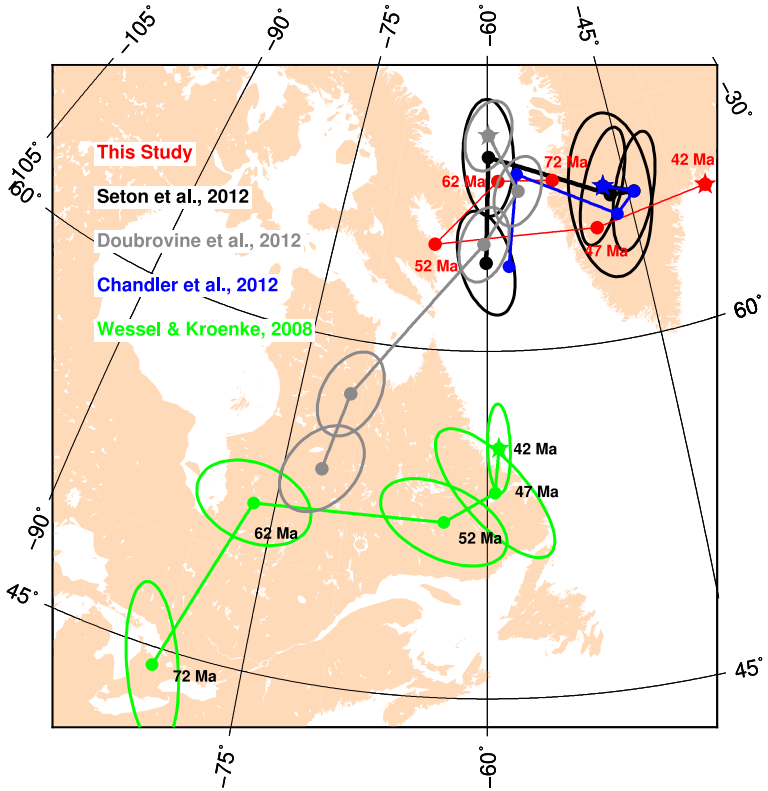

Fig. 6. Finite rotation Euler pole locations for the Pacific Plate at each of the model times. The five different models are coloured as in the legend. Stars represent the 42 Ma Euler poles and progressive points are the 47, 52, 62, and 72 Ma poles, these are only labelled for our model and the Wessel and Kroenke (2008) reconstructions for clarity. Present day continents are overlain in peach for reference. The BEM-Earth Euler poles are the addition of the finite poles from Seton et al. (2012) and the stage rotations of each model run. Projected error ellipses are determined from each source's published covariance matrix.

SED
6, 145–190, 2014

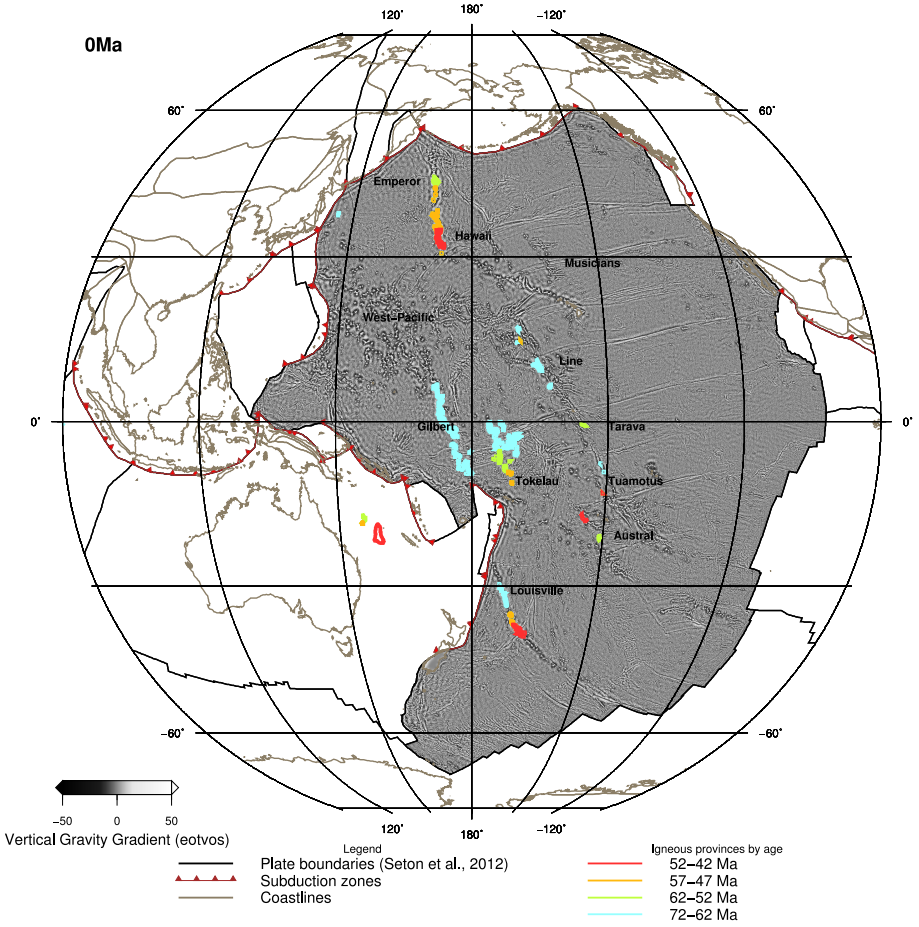

Fig. 7. Present day vertical gravity gradient of the Paficic Plate (Sandwell and Smith, 2009). Present day locations of volcanics dated between 72 and 42 Ma are binned in 10 Myr increments and coloured as in the legend.

SED
6, 145–190, 2014

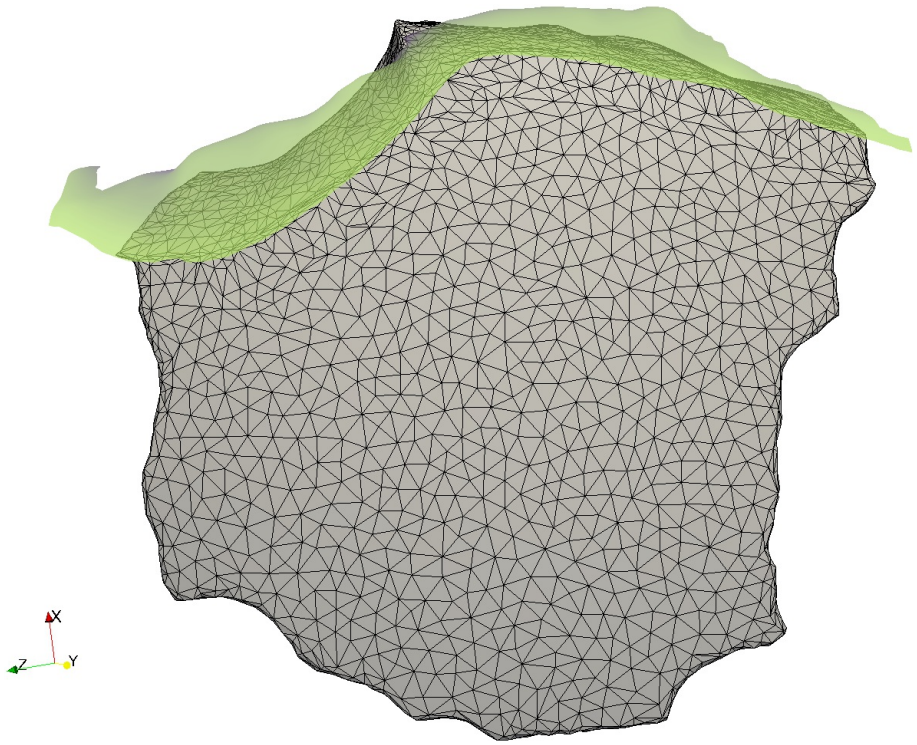

Fig. A1. Top-down view of the Nazca Plate at present day for geodynamic model input. The green to purple colored topology represents the depth of the Nazca slab from the Slab1.0 (Hayes et al., 2012) interpretation. The black mesh over the plate indicates the resolution of the model. The Slab1.0 interpretation is made slightly transparent to see the extent of modelled plate.

SED
6, 145–190, 2014

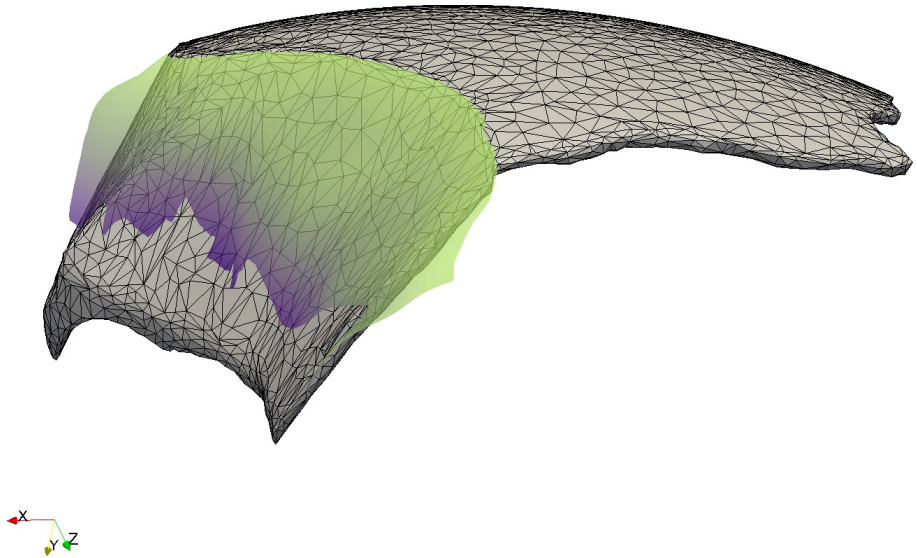

Fig. A2. North side view of the Nazca Plate at present day for geodynamic model input. The green to purple colored topology represents the depth of the Nazca slab from the Slab1.0 (Hayes et al., 2012) interpretation. The black mesh over the plate indicates the resolution of the model. The Slab1.0 interpretation is made slightly transparent to see the extent of modelled plate.

SED
6, 145–190, 2014

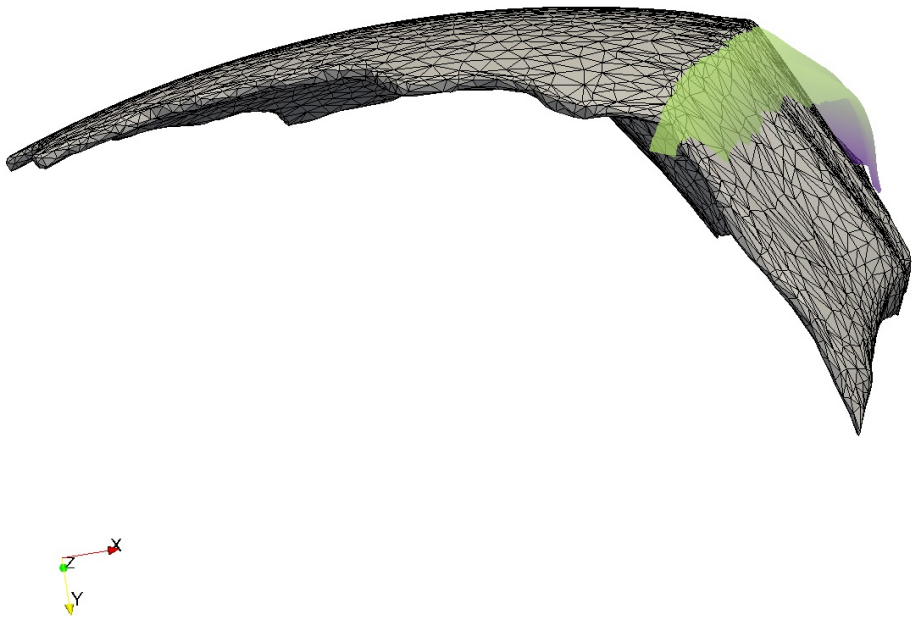

Fig. A3. South side view of the Nazca Plate at present day for geodynamic model input. The green to purple colored topology represents the depth of the Nazca slab from the Slab1.0 (Hayes et al., 2012) interpretation. The black mesh over the plate indicates the resolution of the model. The Slab1.0 interpretation is made slightly transparent to see the extent of modelled plate.

SED
6, 145–190, 2014

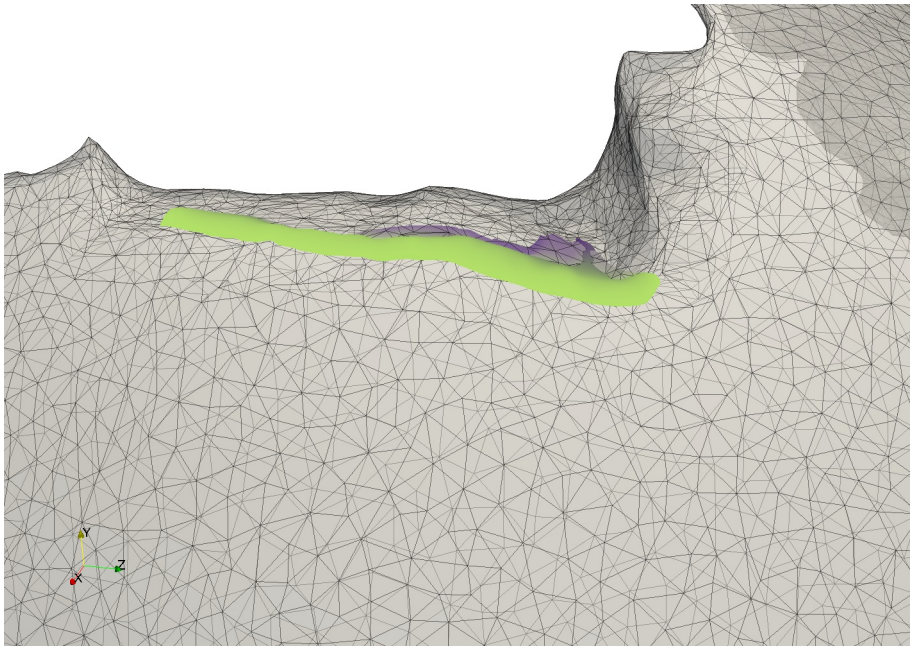

Fig. A4. Top-down view of the Pacific Plate at present day for geodynamic model input, localized over the Tonga-Kermadec subduction zone. The green to purple colored topology represents the depth of the Kermadec slab from the Slab1.0 (Hayes et al., 2012) interpretation. The black mesh over the plate indicates the resolution of the model. The modelled plate is made slightly transparent to see the extent of the Slab1.0 interpretation.

SED
6, 145–190, 2014

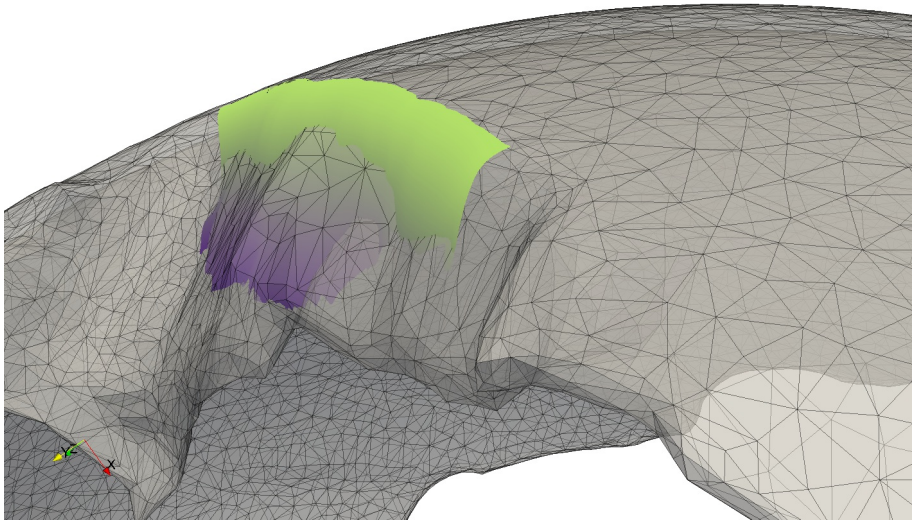

Fig. A5. Side view of the Pacific Plate at present day for geodynamic model input, looking from the south at the Tonga-Kermadec subduction zone. The green to purple colored topology represents the depth of the Kermadec slab from the Slab1.0 (Hayes et al., 2012) interpretation. The black mesh over the plate indicates the resolution of the model. The modelled plate is made slightly transparent to see the extent of the Slab1.0 interpretation.

SED
6, 145–190, 2014

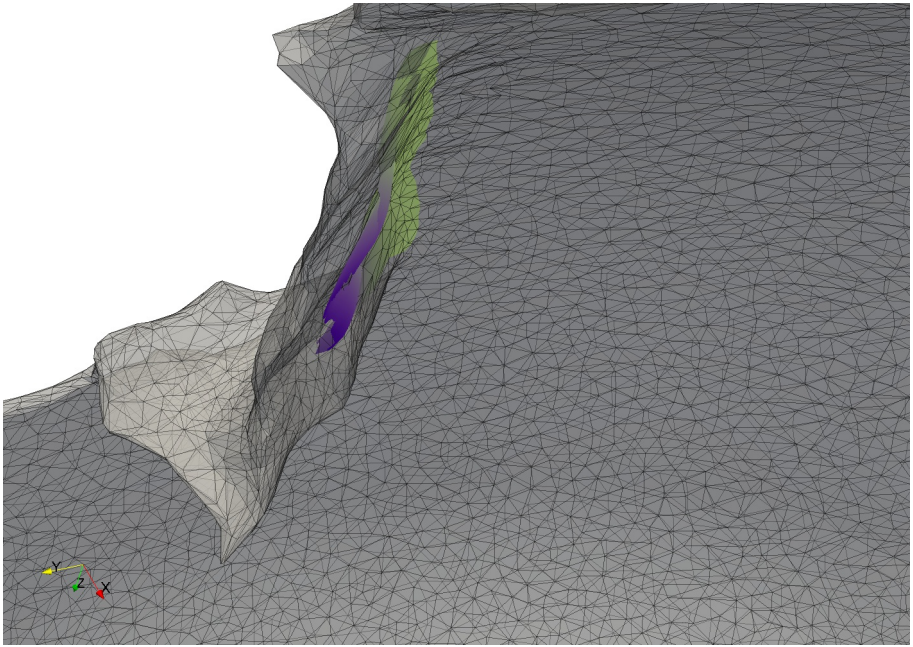

Fig. A6. View of the Pacific Plate at present day for geodynamic model input, looking from beneath the plate at the Tonga-Kermadec subduction zone. The green to purple colored topology represents the depth of the Kermadec slab from the Slab1.0 (Hayes et al., 2012) interpretation. The black mesh over the plate indicates the resolution of the model.

SED
6, 145–190, 2014

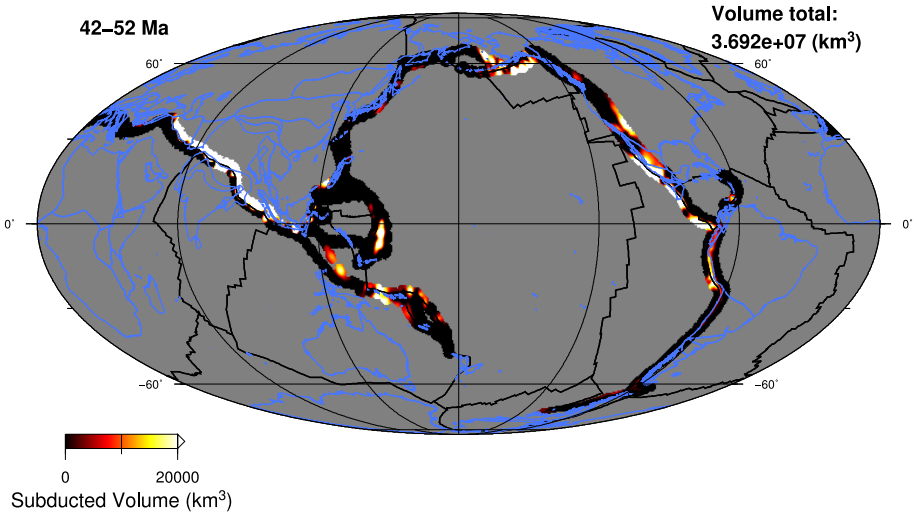

Fig. B1. Integrated volume of subducted material between 52 and 42 Ma. The color scale represents the volume of material. The total amount of material for this time period is 3.7×10^7 km^3.

SED
6, 145–190, 2014

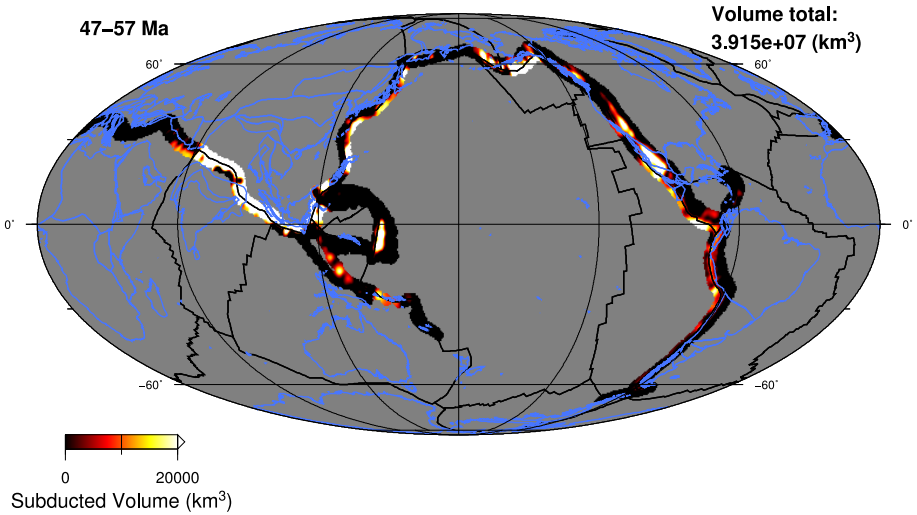

Fig. B2. Integrated volume of subducted material between 57 and 47 Ma. The color scale represents the volume of material. The total amount of material for this time period is 3.9×10^7 km^3.

SED
6, 145–190, 2014

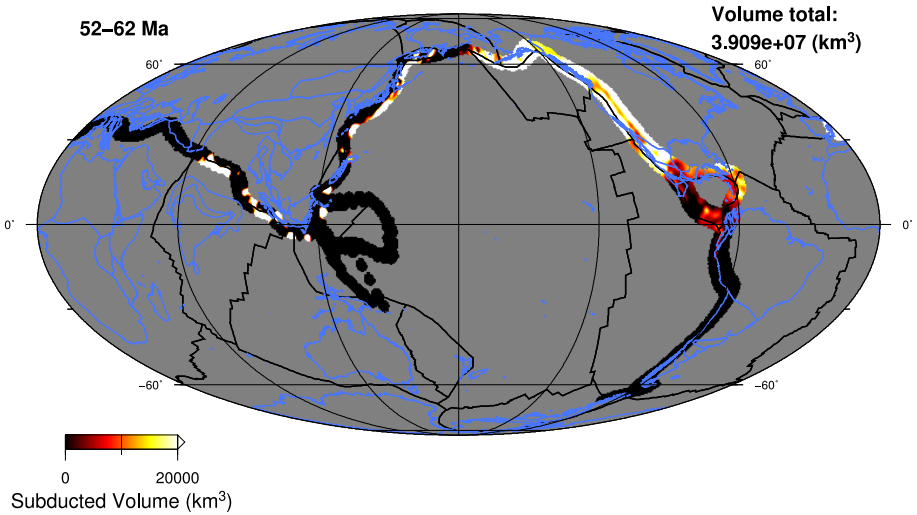

Fig. B3. Integrated volume of subducted material between 62 and 52 Ma. The color scale represents the volume of material. The total amount of material for this time period is 3.9×10^7 km^3.

SED
6, 145–190, 2014

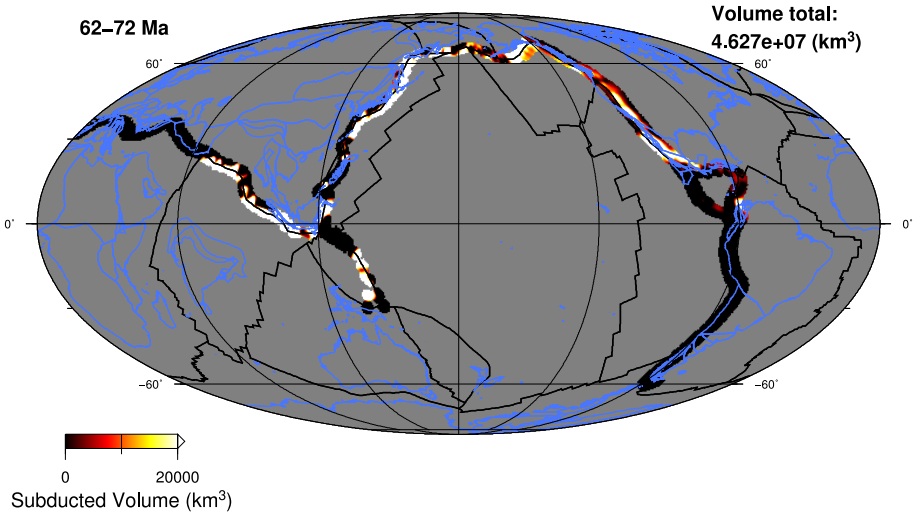

Fig. B4. Integrated volume of subducted material between 72 and 62 Ma. The color scale represents the volume of material. The total amount of material for this time period is 4.6×10^7 km^3.

SED
6, 145–190, 2014